



**Calibration of Smart Weapon Motion Sensors for
High-Speed Manufacturing Lines**

by Delvin Peterson and Mark Costello

ARL-CR-567

September 2005

prepared by

**Oregon State University
Corvallis, OR 97331**

**under contract
W911QX-04-P-0270**

NOTICES

Disclaimers

The findings in this report are not to be construed as an official Department of the Army position unless so designated by other authorized documents.

Citation of manufacturer's or trade names does not constitute an official endorsement or approval of the use thereof.

Destroy this report when it is no longer needed. Do not return it to the originator.

Army Research Laboratory

Aberdeen Proving Ground, MD 21005-5066

ARL-CR-567

September 2005

Calibration of Smart Weapon Motion Sensors for High-Speed Manufacturing Lines

**Delvin Peterson and Mark Costello
Oregon State University**

prepared by

**Oregon State University
Corvallis, OR 97331**

**under contract
W911QX-04-P-0270**

REPORT DOCUMENTATION PAGE			Form Approved OMB No. 0704-0188		
Public reporting burden for this collection of information is estimated to average 1 hour per response, including the time for reviewing instructions, searching existing data sources, gathering and maintaining the data needed, and completing and reviewing the collection information. Send comments regarding this burden estimate or any other aspect of this collection of information, including suggestions for reducing the burden, to Department of Defense, Washington Headquarters Services, Directorate for Information Operations and Reports (0704-0188), 1215 Jefferson Davis Highway, Suite 1204, Arlington, VA 22202-4302. Respondents should be aware that notwithstanding any other provision of law, no person shall be subject to any penalty for failing to comply with a collection of information if it does not display a currently valid OMB control number. PLEASE DO NOT RETURN YOUR FORM TO THE ABOVE ADDRESS.					
1. REPORT DATE (DD-MM-YYYY) September 2005		2. REPORT TYPE Final		3. DATES COVERED (From - To) October 2003–September 2004	
4. TITLE AND SUBTITLE Calibration of Smart Weapon Motion Sensors for High-Speed Manufacturing Lines				5a. CONTRACT NUMBER W911QX-04-P-0270	
				5b. GRANT NUMBER	
				5c. PROGRAM ELEMENT NUMBER	
6. AUTHOR(S) Delvin Peterson * and Mark Costello †				5d. PROJECT NUMBER 622618.H8000	
				5e. TASK NUMBER	
				5f. WORK UNIT NUMBER	
7. PERFORMING ORGANIZATION NAME(S) AND ADDRESS(ES) Oregon State University Corvallis, OR 97331				8. PERFORMING ORGANIZATION REPORT NUMBER	
9. SPONSORING/MONITORING AGENCY NAME(S) AND ADDRESS(ES) U.S. Army Research Laboratory ATTN: AMRSD-ARL-WM-BC Aberdeen Proving Ground, MD 21005-5066				10. SPONSOR/MONITOR'S ACRONYM(S)	
				11. SPONSOR/MONITOR'S REPORT NUMBER(S) ARL-CR-567	
12. DISTRIBUTION/AVAILABILITY STATEMENT Approved for public release; distribution is unlimited.					
13. SUPPLEMENTARY NOTES * Graduate Research Assistant, Department of Mechanical Engineering, Oregon State University † Associate Professor, Department of Mechanical Engineering, Oregon State University					
14. ABSTRACT Accelerometers and gyroscopes are used in many smart weapon sensor suites. If dominant sensor error sources such as misposition, bias, cross axis sensitivity, and scale factor can be quickly and efficiently identified and loaded onto the sensor suites, quality feedback can be achieved at significant cost savings. The work reported here describes a relatively simple sensor calibration device suitable for a high volume production line environment. It consists of a freely vibrating table supported by a ball and socket joint in the middle and springs on the corners of the platform. Robotic devices are rigidly fastened to the vibrating table. Table orientation is measured with a six-camera, motion-capture system. Sensor suite and table orientation data are blended together in an extended Kalman filter to estimate accelerometer and gyroscope bias, cross axis sensitivity, and scale factor, along with accelerometer misposition. Experimental results indicate that a two-phase procedure including static and dynamic conditions was found to be most successful at identifying all calibration constants.					
15. SUBJECT TERMS guided projectile, divert control, unbalanced part					
16. SECURITY CLASSIFICATION OF:			17. LIMITATION OF ABSTRACT UL	18. NUMBER OF PAGES 32	19a. NAME OF RESPONSIBLE PERSON Peter Plostins
a. REPORT UNCLASSIFIED	b. ABSTRACT UNCLASSIFIED	c. THIS PAGE UNCLASSIFIED			19b. TELEPHONE NUMBER (Include area code) 410-278-8878

Contents

List of Figures	iv
List of Tables	iv
1. Introduction	1
2. Table Dynamic Model	3
3. Sensor Readings	5
4. Measurement System	7
5. Estimation Technique	8
6. Model Parameter Estimation	9
7. Sensor Error Results	10
8. Conclusions	19
9. References	21
List of Symbols, Abbreviations, and Acronyms	23
Distribution List	25

List of Figures

Figure 1. Calibration table.	2
Figure 2. Reference frame.....	3
Figure 3. Oregon State University motion capture laboratory.....	7
Figure 4. Roll angle vs. time. Solid = measured data; dashed = updated simulation; dotted = original simulation.	11
Figure 5. Pitch angle vs. time. Solid = measured data; dashed = updated simulation; dotted = original simulation.	11
Figure 6. Yaw angle vs. time. Solid = measured data; dashed = updated simulation; dotted = original simulation.	12
Figure 7. Static table orientation 1.....	12
Figure 8. Static table orientation 2.....	13
Figure 9. Accelerometer bias.	13
Figure 10. Accelerometer scale factors.....	14
Figure 11. Accelerometer cross-axis sensitivities.....	14
Figure 12. Rate gyro bias.	15
Figure 13. Static phase acceleration errors.	15
Figure 14. Static phase angular velocity errors.....	16
Figure 15. Accelerometer mispositions.	17
Figure 16. Rate gyro scale factors.....	17
Figure 17. Rate gyro cross-axis sensitivities.....	18
Figure 18. Dynamic phase acceleration errors.....	18
Figure 19. Dynamic phase angular velocity errors.	19

List of Tables

Table 1. Model parameters.	10
Table 2. Sensor error parameter comparison.	20

1. Introduction

Accelerometers and gyroscopes are used in navigational control of various devices including smart weapons. While these sensors are available in varying degrees of accuracy, it is significantly less expensive to use lower accuracy sensors. If sensor error sources including misposition, bias, cross axis sensitivity, and scale factor can be identified and recorded, quality feedback can be achieved at significant cost savings. Moreover, to decrease production cost, calibration of sensor suites must be accomplished in a cost effective manner leading to the need for mass-manufacturing techniques to be applied to the calibration procedure.

Calibration of sensors used in navigational control is accomplished using various methods. For instance, Costello and Erickson (1) describe a theoretical method for calibrating an inertial measuring device using a Kalman filter on a simulated vibrating table. Grewal et al. (2) describe an application of the Kalman filter to calibration of an inertial navigation system with a large error state vector. Also, Kim and Golnaraghi (3) propose an optical position tracking system which is used to calibrate a moving sensor suite. Leach and Hui (4) write about a calibration system that is performed in flight by an aircraft performing a sequence of turns. Similarly, Nebot and Durrant-Whyte (5) describe a calibration system for accelerometers and gyroscopes based on motion developed by driving a land vehicle. Haessig and Friedland (6) describe a two-stage Kalman filter which separates bias errors from the other states. A deterministic correlation identification method to calibrate accelerometer with drifting bias is explained by Hung et al. (7).

The work reported here describes a simple sensor calibration technique suitable for high volume production line environments. A vibrating table, supported at the center by a ball-and-socket joint and at the four corners by springs, is used to develop motion for calibration. Springs cause the system to oscillate around the equilibrium position until the motion is damped by inherent friction in the springs and gimbal joint. Table motion is pure rotation about the pivot point of the gimbal joint, so the table possesses three rotational degrees of freedom. A picture of the calibration table is shown in figure 1.

During the calibration procedure, orientation of the calibration table is measured with a six-camera, motion-capture system. Single-axis accelerometers and gyroscopes are mounted inside the robotic devices and each is attached at known locations on the vibrating table. These sensors constitute the core sensors of a conventional inertial measurement unit (IMU). In order to blend with mass production, sensor calibration is one of the final steps in the production sequence after the IMU has been fixed to the device that is to be controlled. Once calibration parameters are determined they are uploaded to the microprocessor.

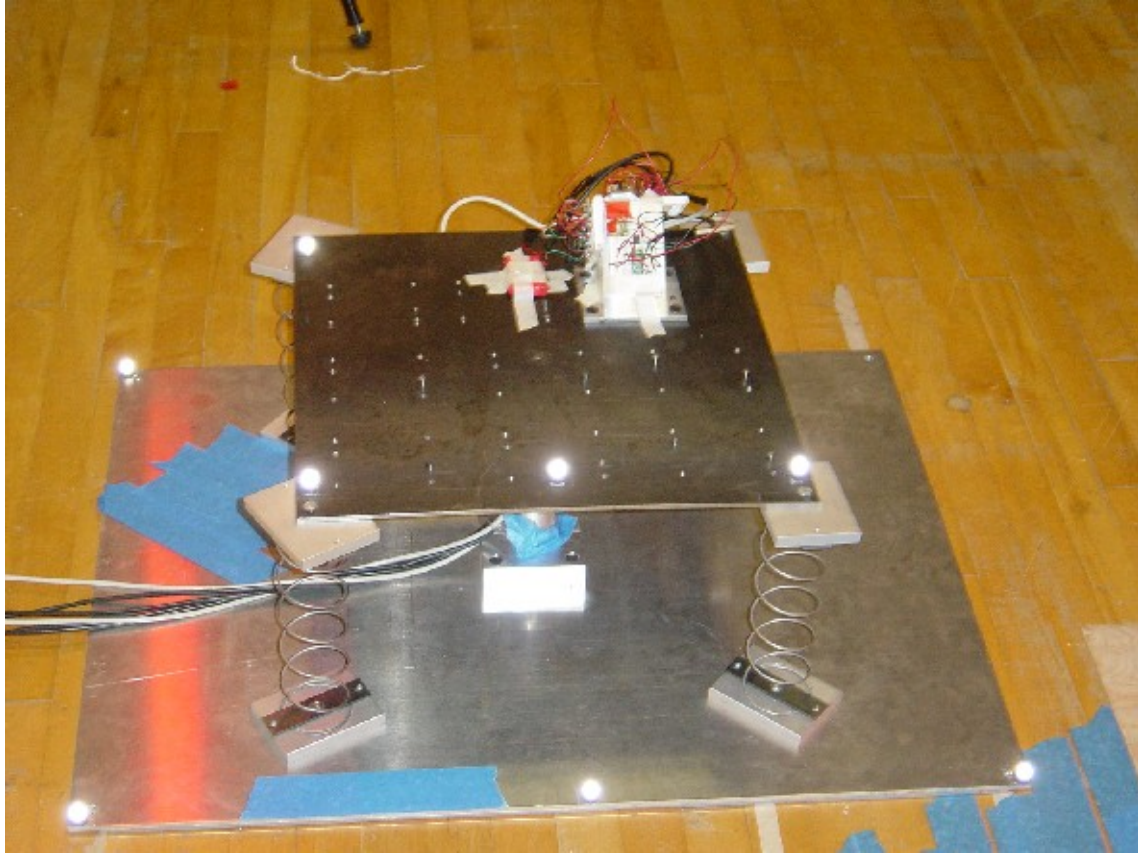


Figure 1. Calibration table.

The proposed calibration procedure is a two-step process including a static phase and a dynamic phase. In the static phase, sensor readings are measured at each of a series of fixed table orientations. Based on the sensor readings and the orientations of the table, parameters that can be estimated without table motion are identified. With the static parameters fixed, the remaining parameters are estimated based on dynamically oscillating table motion during the dynamic phase. Note that no actuators are required for the dynamic phase because sufficient table motion is generated by simply deflecting the table from its equilibrium position and releasing the table so that it enters a state of free vibration.

To demonstrate the utility of this system, the technique is experimentally tested by using the two-step sequence to estimate calibration parameters with sensors at different locations and orientations. By comparing prior misposition and misalignment parameters to changes estimated by the calibration method, accuracy is determined. The technique is shown to be a viable technique for quick batch calibration of motion sensors on small robotic devices.

2. Table Dynamic Model

The table shown in figure 1 is modeled as a rigid body that rotates about a gimbal joint. The table possesses three orientation degrees of freedom. The I frame is fixed to the ground and the B frame is fixed to the vibrating table, as shown in figure 2. Orientation of the table is described by a series of three body-fixed rotations from the inertial frame (8). First, frame O is obtained by rotating by an angle ψ about \vec{K}_I . Next, frame O is rotated about \vec{J}_O by an angle θ to obtain frame T . Finally, the body frame B is obtained by a ϕ rotation about \vec{I}_T . The angles ϕ, θ , and ψ are the Euler angles used as three of the six states for developing the equations of motion. Based on this rotation scheme, the inertial and body frame unit vectors are related by the rotation matrix,

$$\begin{Bmatrix} \vec{I}_B \\ \vec{J}_B \\ \vec{K}_B \end{Bmatrix} = \begin{bmatrix} c_\theta c_\psi & c_\theta s_\psi & -s_\theta \\ -c_\phi s_\psi + s_\phi s_\theta c_\psi & c_\phi c_\psi + s_\phi s_\theta s_\psi & s_\phi c_\theta \\ s_\phi s_\psi + c_\phi s_\theta c_\psi & -s_\phi c_\psi + c_\phi s_\theta s_\psi & c_\phi c_\theta \end{bmatrix} \begin{Bmatrix} \vec{I}_I \\ \vec{J}_I \\ \vec{K}_I \end{Bmatrix} = [R] \begin{Bmatrix} \vec{I}_I \\ \vec{J}_I \\ \vec{K}_I \end{Bmatrix}, \quad (1)$$

using the shorthand notation: $s_\alpha \equiv \sin \alpha$, $c_\alpha \equiv \cos \alpha$, and $t_\alpha \equiv \tan \alpha$.

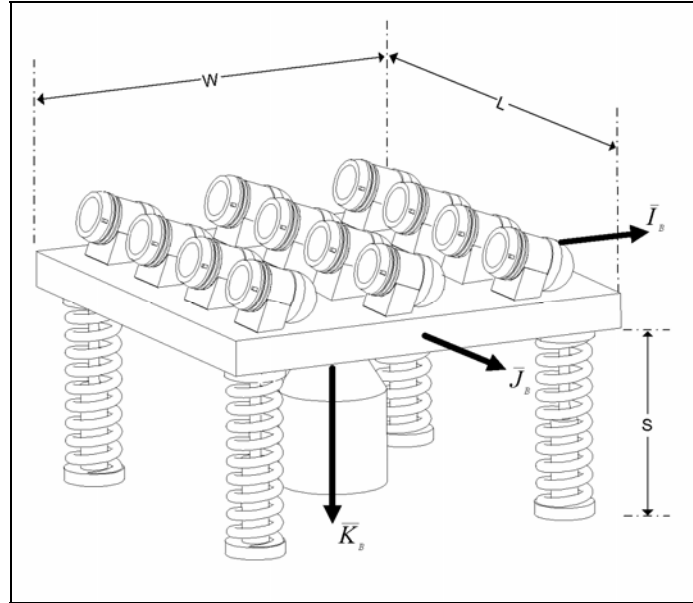


Figure 2. Reference frame.

The remaining three state variables are chosen as the components of the angular velocity vector of the table expressed in the body frame.

$$\vec{\omega}_{B/I} = p\bar{I}_B + q\bar{J}_B + r\bar{K}_B. \quad (2)$$

The kinematic differential equations are formed by equating the angular velocity using the previous equation and using time rates of change of Euler angles.

$$\begin{Bmatrix} \dot{\phi} \\ \dot{\theta} \\ \dot{\psi} \end{Bmatrix} = \begin{bmatrix} 1 & s_\phi t_\theta & c_\phi t_\theta \\ 0 & c_\phi & -s_\phi \\ 0 & s_\phi/c_\theta & c_\phi/c_\theta \end{bmatrix} \begin{Bmatrix} p \\ q \\ r \end{Bmatrix}. \quad (3)$$

The kinetic equations of motion are developed using Newtonian mechanics.

$$m\vec{a}_{\oplus/I} = \vec{W} + \vec{F}_R + \sum_{i=1}^4 \vec{F}_{Si} + \sum_{i=1}^4 \vec{F}_{Di}. \quad (4)$$

$$\frac{{}^I d\vec{H}_{B/I}^\oplus}{dt} = \vec{M}_f + \sum_{i=1}^4 \vec{T}_{Si} + \vec{r}_{\oplus \rightarrow P} \times \vec{F}_R + \sum_{i=1}^4 \vec{r}_{\oplus \rightarrow Si} \times (\vec{F}_{Si} + \vec{F}_{Di}). \quad (5)$$

Using equation 4 to solve for \vec{F}_R and subsequently substituting into equation 5 yields the following equations of motion expressed in components of frame B .

$$\begin{Bmatrix} \dot{p} \\ \dot{q} \\ \dot{r} \end{Bmatrix} = [\bar{I}]^{-1} \begin{pmatrix} \sum_{i=1}^4 (S_B(\vec{r}_{P \rightarrow Ti})(\vec{F}_{Si} + \vec{F}_{Di}) + \vec{T}_{Si}) + S_B(\vec{r}_{P \rightarrow \oplus})\vec{W} + \vec{M}_f \\ + mS_B(-\vec{r}_{P \rightarrow \oplus})S_B(\vec{\omega}_{B/I})^2 S_B(\vec{r}_{P \rightarrow \oplus}) - S_B(\vec{\omega}_{B/I})[I]S_B(\vec{\omega}_{B/I}) \end{pmatrix}, \quad (6)$$

where

$$[\bar{I}] = [I] - m \begin{bmatrix} -r_y^2 - r_z^2 & r_x r_y & r_x r_z \\ r_x r_y & -r_x^2 - r_z^2 & r_y r_z \\ r_x r_z & r_y r_z & -r_x^2 - r_y^2 \end{bmatrix}.$$

The spring forces are obtained by:

$$\begin{Bmatrix} F_{Six} \\ F_{Siy} \\ F_{Siz} \end{Bmatrix} = k \frac{|\vec{r}_{Ti \rightarrow Fi}| - s_0}{|\vec{r}_{Ti \rightarrow Fi}|} \begin{Bmatrix} r_{TFix} \\ r_{TFiy} \\ r_{TFiz} \end{Bmatrix}, \quad (7)$$

where

$$C_B(\vec{r}_{Ti \rightarrow Fi}) = \begin{Bmatrix} r_{TFix} \\ r_{TFiy} \\ r_{TFiz} \end{Bmatrix} = - \begin{Bmatrix} r_{PTix} \\ r_{PTiy} \\ r_{PTiz} \end{Bmatrix} - [R] \begin{Bmatrix} r_{FPix} \\ r_{FPiy} \\ r_{FPiz} \end{Bmatrix}.$$

In the same manner, the damping forces are given by

$$\begin{Bmatrix} F_{Dix} \\ F_{Diy} \\ F_{Diz} \end{Bmatrix} = \frac{c}{|\vec{r}_{Ti \rightarrow Fi}|^2} \begin{Bmatrix} r_{TFix} \\ r_{TFiy} \\ r_{TFiz} \end{Bmatrix} \bullet \frac{d}{dt} [R] \begin{Bmatrix} r_{FPix} \\ r_{FPiy} \\ r_{FPiz} \end{Bmatrix} \begin{Bmatrix} r_{TFix} \\ r_{TFiy} \\ r_{TFiz} \end{Bmatrix}. \quad (8)$$

The i^{th} spring torsional moment is

$$\vec{T}_{Si} = -k_t \psi \bar{K}_B. \quad (9)$$

Also, the weight force is

$$\vec{W} = mg \bar{K}_I = mg \left(-s_\theta \bar{I}_B + s_\phi c_\theta \bar{J}_B + c_\phi c_\theta \bar{K}_B \right). \quad (10)$$

Finally, the joint frictional moment is

$$\vec{M}_f = -b_f \vec{\omega}_{B/I}. \quad (11)$$

Since the table is a freely oscillating system, there is no input to the system. The state dynamic equations can be expressed in the form $\dot{\vec{x}} = \vec{f}(\vec{x})$. These equations are used to predict the motion of the table to optimize the error-estimation algorithm.

3. Sensor Readings

Within the Kalman filter estimator, measured motion of the table is contrasted with accelerometer and gyroscope measurements to iteratively determine sensor calibration parameters. To properly blend this data, accelerometer and gyroscope measurements are related to table motion. This link is created using rigid body kinematics. The acceleration experienced by the location of an accelerometer is

$$\vec{a}_{Si/I} = \vec{\alpha}_{B/I} \times \vec{r}_{P \rightarrow Si} + \vec{\omega}_{B/I} \times (\vec{\omega}_{B/I} \times \vec{r}_{P \rightarrow Si}), \quad (12)$$

or, in component form in the sensor reference frame,

$$S_S(\vec{a}_{Si/I}) = [R_S][S]S_B(\vec{r}_{P \rightarrow Si}), \quad (13)$$

where $[S] = S_B(\vec{\alpha}_{B/I}) + S_B(\vec{\omega}_{B/I})S_B(\vec{\omega}_{B/I})$.

Also, the angular velocity of the gyroscopes is

$$\vec{\omega}_{Si/I} = \vec{\omega}_{B/I} \Rightarrow S_S(\vec{\omega}_{Si/I}) = [R_S] \begin{Bmatrix} p \\ q \\ r \end{Bmatrix}. \quad (14)$$

Note that angular velocity and linear acceleration components given in equations 13 and 14 are expressed in a reference frame aligned with a reference frame along the sensor. The transformation matrix from vector components in frame B to vector components in frame S is given by R_s . Major error sources of accelerometers and gyroscopes are bias error, scale factor error, and cross-axis sensitivity/misalignment. Sensor misposition is also an important error source for accelerometers. For rigid bodies, misposition does not affect the gyroscope readings since angular velocity is a body property not a point property. Also, cross-axis sensitivity and misalignment are indistinguishable so they are lumped together. Accelerometers are affected by gravity as well as acceleration. Including these error sources, an accelerometer reading during the dynamic phase is described by

$$a_i = a_{Bi} + [S_A][R_S] \left([S] \left(C_B(\vec{r}_{P \rightarrow Si}) + \begin{Bmatrix} \delta_{Si}^x \\ \delta_{Si}^y \\ \delta_{Si}^z \end{Bmatrix} \right) - g \begin{Bmatrix} -s_\theta \\ s_\phi c_\theta \\ c_\phi c_\theta \end{Bmatrix} \right), \quad (15)$$

where

$$[S_A] = \begin{bmatrix} s_{Ax} & c_{Ax}^y & c_{Ax}^z \\ c_{Ay}^x & s_{Ay} & c_{Ay}^z \\ c_{Az}^x & c_{Az}^y & s_{Az} \end{bmatrix}.$$

In the same manner, a gyroscope reading is expressed as

$$\begin{Bmatrix} \omega_x \\ \omega_y \\ \omega_z \end{Bmatrix} = \begin{Bmatrix} \omega_{Bx} \\ \omega_{By} \\ \omega_{Bz} \end{Bmatrix} + \begin{bmatrix} s_{Gx} & c_{Gx}^y & c_{Gx}^z \\ c_{Gy}^x & s_{Gy} & c_{Gy}^z \\ c_{Gz}^x & c_{Gz}^y & s_{Gz} \end{bmatrix} [R_S] \begin{Bmatrix} p \\ q \\ r \end{Bmatrix}. \quad (16)$$

During the static phase of parameter estimation, the angular velocity and angular acceleration of the table are neglected. The previous equations simplify to the static sensor readings

$$a_i = a_{Bi} + \vec{s}_{Ai}^T [R_S] g \begin{Bmatrix} s_\theta \\ -s_\phi c_\theta \\ -c_\phi c_\theta \end{Bmatrix}, \quad (17)$$

and

$$\begin{Bmatrix} \omega_x \\ \omega_y \\ \omega_z \end{Bmatrix} = \begin{Bmatrix} \omega_{Bx} \\ \omega_{By} \\ \omega_{Bz} \end{Bmatrix}. \quad (18)$$

Thus, bias errors, scale factors, and cross-axis sensitivities of the accelerometers, as well as bias errors of the gyroscopes, can be estimated during the static phase.

4. Measurement System

A motion-capture camera system is used to measure orientation of the table. A picture of the Oregon State University Motion Capture Laboratory is shown in figure 3. The motion-capture system consists of a set of six 1.2-megapixel visible red cameras coupled together. The cameras are optimized to identify reflective markers that reside within the field of view of the camera. Using three-dimensional (3-D) correlation techniques, the position of each marker is determined within the 3-D measurement volume of the motion-capture system (9).



Figure 3. Oregon State University motion capture laboratory.

Using the location of three reflective markers on a body, orientation of the body is calculated. Two markers are carefully placed along an axis parallel to the \bar{I}_B unit vector. Another marker is placed in a direction parallel to the \bar{J}_B axis from the origin marker. By calculating the difference between both sets of markers, \bar{I}_B and \bar{J}_B are written in terms of Vicon reference frame coordinates (V). Finally \bar{K}_B is found normal to the plane of the table by calculating

$\bar{I}_B \times \bar{J}_B$. A similar procedure is used with markers located on the floor to define the unit vectors of the I frame in the V frame. Substituting the inertial-frame equations into the body-frame equations, the rotation matrix of the table is

$$\begin{Bmatrix} \bar{I}_B \\ \bar{J}_B \\ \bar{K}_B \end{Bmatrix} = [R] \begin{Bmatrix} \bar{I}_I \\ \bar{J}_I \\ \bar{K}_I \end{Bmatrix}, \quad (19)$$

where

$$[R] = [R_{V \rightarrow B}] [R_{V \rightarrow I}]^T.$$

Based on this rotation matrix, the Euler angles ϕ , θ , and ψ are found from equation 1. By numerically differentiating this data using a fourth order finite difference algorithm with a moving average, Euler angle rates and angular accelerations are also determined.

A set of three single-axis accelerometers and three single-axis gyroscopes mounted approximately orthogonal to each other are rigidly attached to the vibrating table to replicate inertial sensors on a small robotic device. The accelerometers are manufactured by Analog Devices (part number ADXL210JE) as are the gyroscopes (part number ADXRS300ABG). The accelerometers are advertised with bias of $\pm 64 \text{ ft/s}^2$, scale factor of 0.85–1.25, and cross axis sensitivity of $\pm 2\%$ (10). The gyroscopes have bias of $\pm 0.7 \text{ rad/s}$, and scale factor of 0.92–1.08 (11). Data from all six sensors is read through an analog-to-digital converter and time stamped with marker position data so that at any given time instant, table orientation and angular velocity, as well as the sensor readings, are known. Data is sampled at a frequency of 500 Hz. Both sensor data and table-orientation data are filtered using a low-pass digital filter with a cutoff frequency of 15 Hz for the dynamic phase. For static phase readings, the data is averaged over a 5-s time increment to remove noise.

5. Estimation Technique

An extended Kalman filter is used to estimate sensor parameters. This method is a five-step process to iteratively estimate a set of states based on weighing the reliability of actual output vs. the observer estimate of the output (12). The Kalman states are the error parameters including the bias for all six sensors, cross axis sensitivity in two directions for all six sensors, scale factor for all six sensors, and three coordinates of misposition for all three accelerometers. This is a total of 33 parameters. The Kalman filter iteratively compares the covariance of the system parameters (P_k) with the covariance of the measurements (R_k) to determine whether to rely more on the measurements or the estimated measurements when updating the states. As time progresses and the estimation converges, the system covariance decreases such that the Kalman filter relies mainly on the model rather than the measurements. To prevent the system

covariance from decreasing such that the filter relies too heavily on the estimated states and discards sensor measurements, model noise is added to the state covariance at each time step.

The first and second steps in this process are projecting the state and error covariance forward in time. Since estimated parameters are constant,

$$\hat{x}_k^- = \hat{x}_{k-1}. \quad (20)$$

$$P_k^- = P_{k-1} + Q_{k-1}. \quad (21)$$

Computing the Kalman gain is the third step in the process:

$$K_k = P_k^- C_k^T (C_k P_k^- C_k^T + R_k)^{-1}, \quad (22)$$

where C_k is the Jacobian of the system of equations describing the output with respect to the states.

$$z_k = z(x_k) + v_k. \quad (23)$$

$$z_k = [a_x \quad a_y \quad a_z \quad \omega_x \quad \omega_y \quad \omega_z]^T. \quad (24)$$

When estimating error parameters of the sensors, equations 15 and 16 are used for the output in the dynamic phase. During the static phase, equations 17 and 18 are used. Parameters are updated by

$$\hat{x}_k = \hat{x}_k^- + K_k (z_k - c(\hat{x}_k^-, v_k = 0)), \quad (25)$$

while updating the covariance matrix is governed by

$$P_k = (I - K_k C_k) P_k^-. \quad (26)$$

This process is iterated at each time step to update the error parameters and the state covariance.

6. Model Parameter Estimation

In addition to estimating sensor-error parameters, a separate Kalman filter is used to match the simulated motion with measured motion by estimating system properties of the table model. The table angular acceleration measured from the motion capture system is used as the output for the Kalman filter such that the output equation, $z_k = z(x_k) + v_k$, is given by equation 6. Uncertain model parameters are used as the Kalman states, including: mass and inertia properties; spring coefficients for both linear and torsional motion; spring and gimbal joint damping coefficients; mass center location; and table height above the pivot point. Initially parameters are obtained

from vendor data, calculated from the geometry and masses of the table components, or estimated based on engineering judgment. The Kalman filter is used to update the uncertain parameters by comparing measured angular accelerations to simulated data using the equations of motion. Table 1 displays the values of the model parameters before and after parameter estimation.

Table 1. Model parameters.

Parameter	Initial	Final
Inertia, I_{xx} (slug-ft ²)	0.145439	0.131563
Inertia, I_{yy} (slug-ft ²)	0.147686	0.14621
Inertia, I_{zz} (slug-ft ²)	0.290066	0.28684
Inertia, I_{xy} (slug-ft ²)	-0.00724	-0.00882
Inertia, I_{xz} (slug-ft ²)	0.003272	-0.00107
Inertia, I_{yz} (slug-ft ²)	0.002653	0.003763
Mass, m (slug)	0.668752	0.659039
Spring stiff, k (lb/ft)	24	22.3299
Spring damping, c (lb/(ft/s))	0.01	0.005828
Tors. spring stiff, k_s (lb-ft/rad)	5	4.050551
Gimbal damping, b_f (lb-ft/(rad/s))	0.1	0.083836
Mass center, r_x (ft)	0.035762	0.042811
Mass center, r_y (ft)	0.030704	0.04203
Mass center, h_c (ft)	0.017487	0.019474
Pivot height, d_{PT} (ft)	0.1875	0.164529

Using a Kalman filter to estimate the model parameters of the simulated vibrating table improves the accuracy of the simulation. As is shown in figures 4–6, the simulation results with estimated parameters matches experimental data closer than simulation results with initial parameters. A perfect match is not achieved; however a perfect match is not possible because the model is not complete and relies on simplifying assumptions. However, since the equations of motion are not directly used in the Kalman filter for the error parameters, the model parameter estimation is adequate to correct the model.

7. Sensor Error Results

Sensor calibration begins with a static phase to estimate bias errors, scale factors, and cross-axis sensitivities of the accelerometers as well as biases of the gyroscopes. Thirty-five table orientations, such as those pictured in figures 7 and 8, are measured and these data are stacked sequentially to provide sufficient data for error parameter convergence. As shown in figures 9–12, the static phase of the Kalman filter allowed all static parameters to converge within 350 static orientations. Bias parameters converge in the least amount of orientations with 50 samples for the accelerometers and 10 samples for the rate gyros. Figures 13 and 14 demonstrate rapid error convergence to the expected sensor errors for the accelerometers and gyroscopes, respectively.

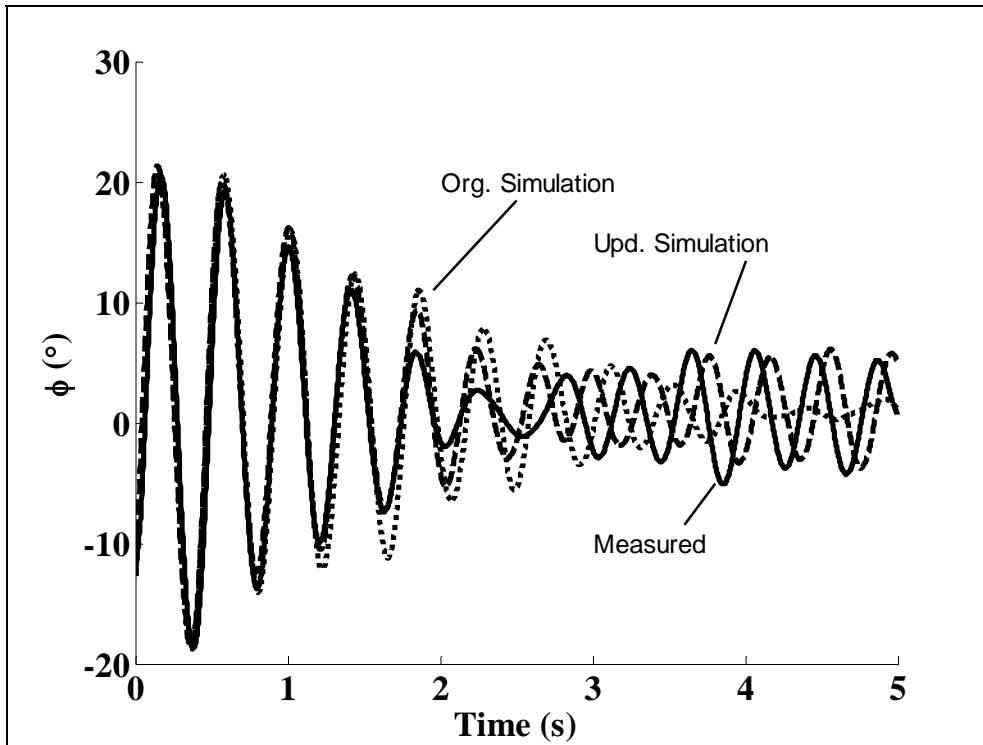


Figure 4. Roll angle vs. time. Solid = measured data; dashed = updated simulation; dotted = original simulation.

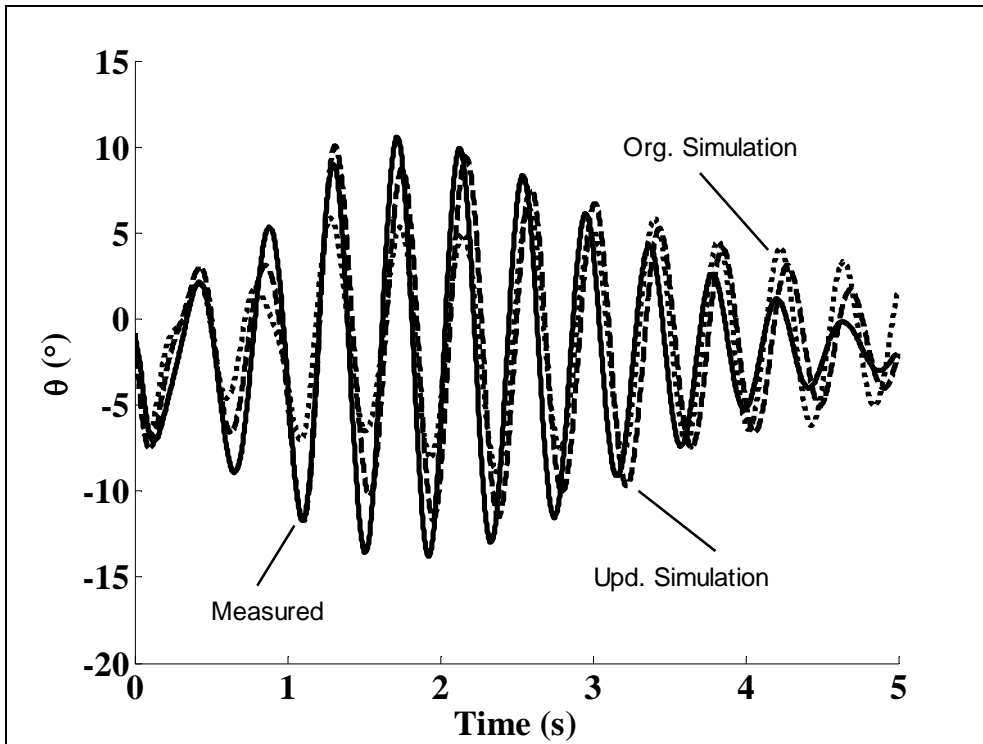


Figure 5. Pitch angle vs. time. Solid = measured data; dashed = updated simulation; dotted = original simulation.

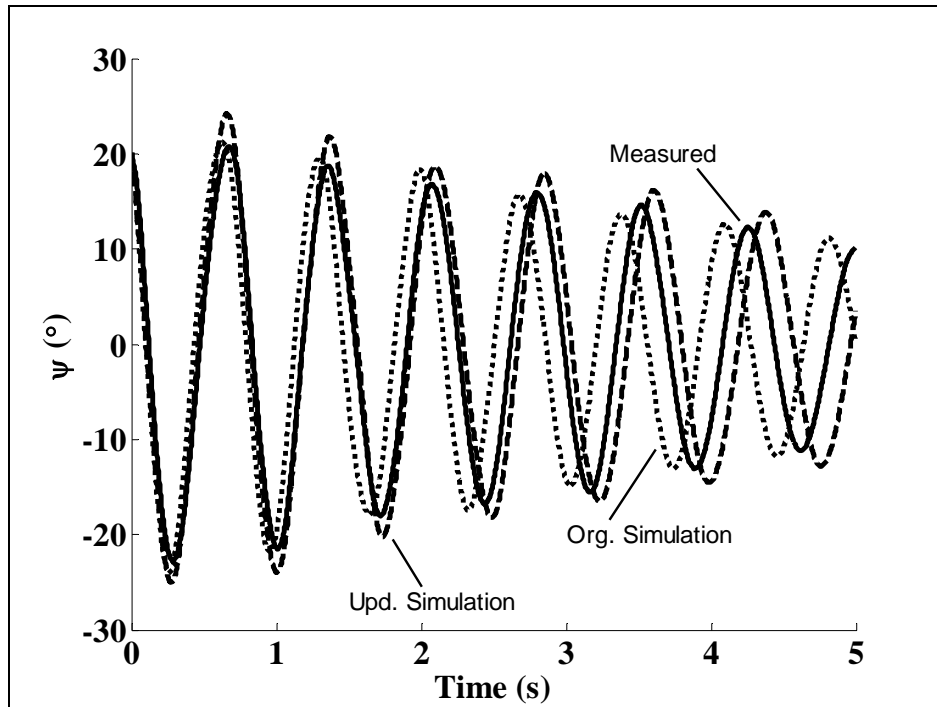


Figure 6. Yaw angle vs. time. Solid = measured data; dashed = updated simulation; dotted = original simulation.

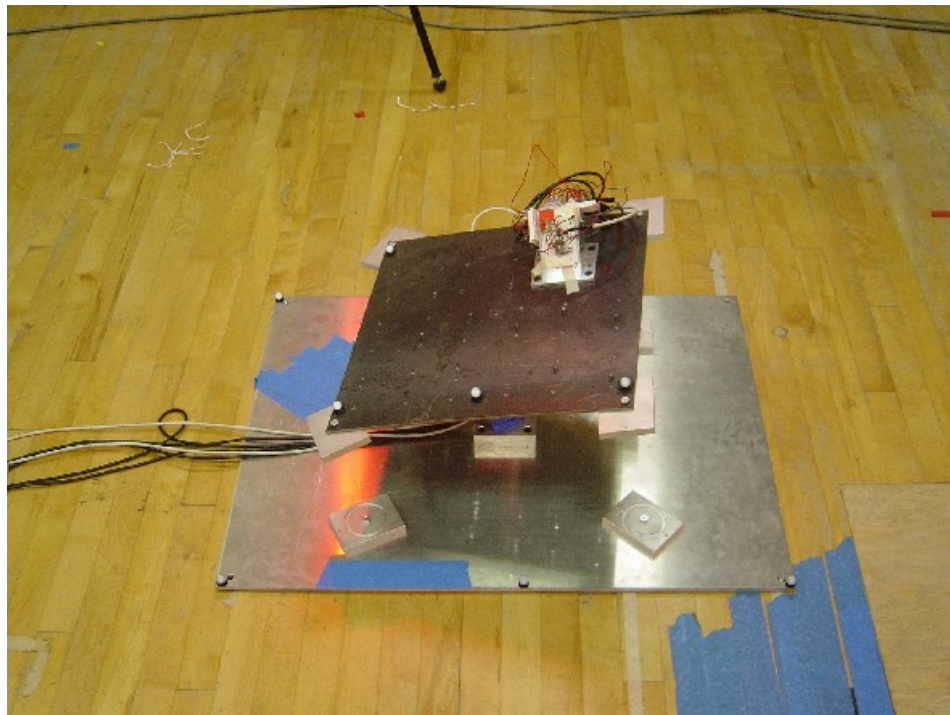


Figure 7. Static table orientation 1.

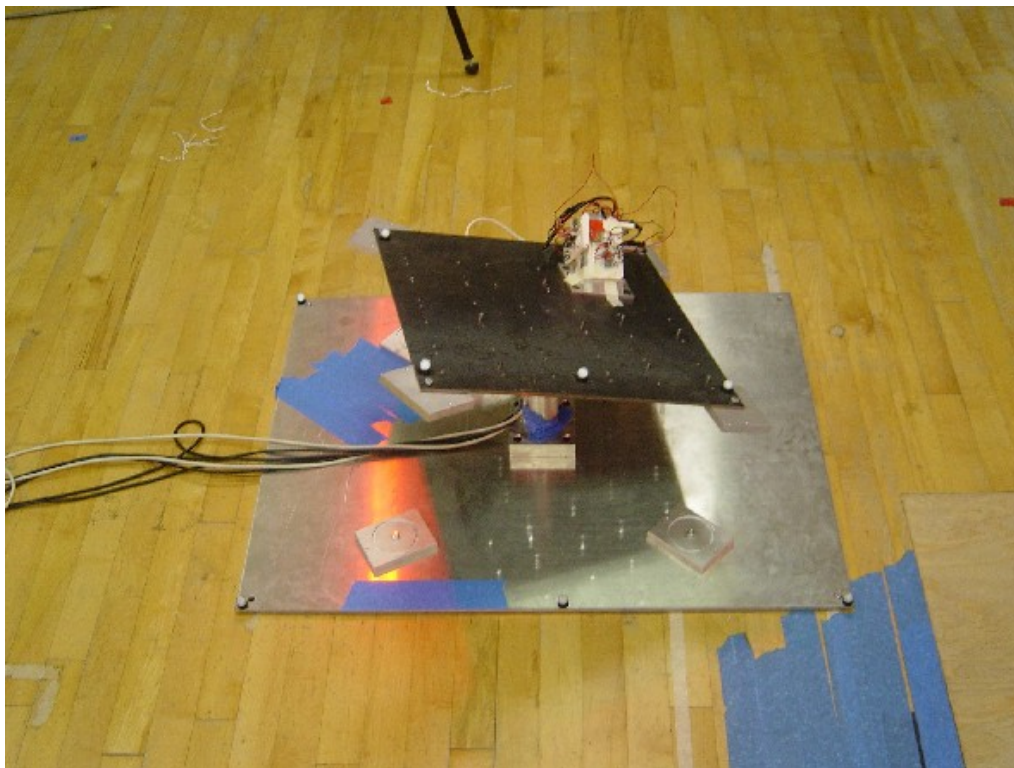


Figure 8. Static table orientation 2.

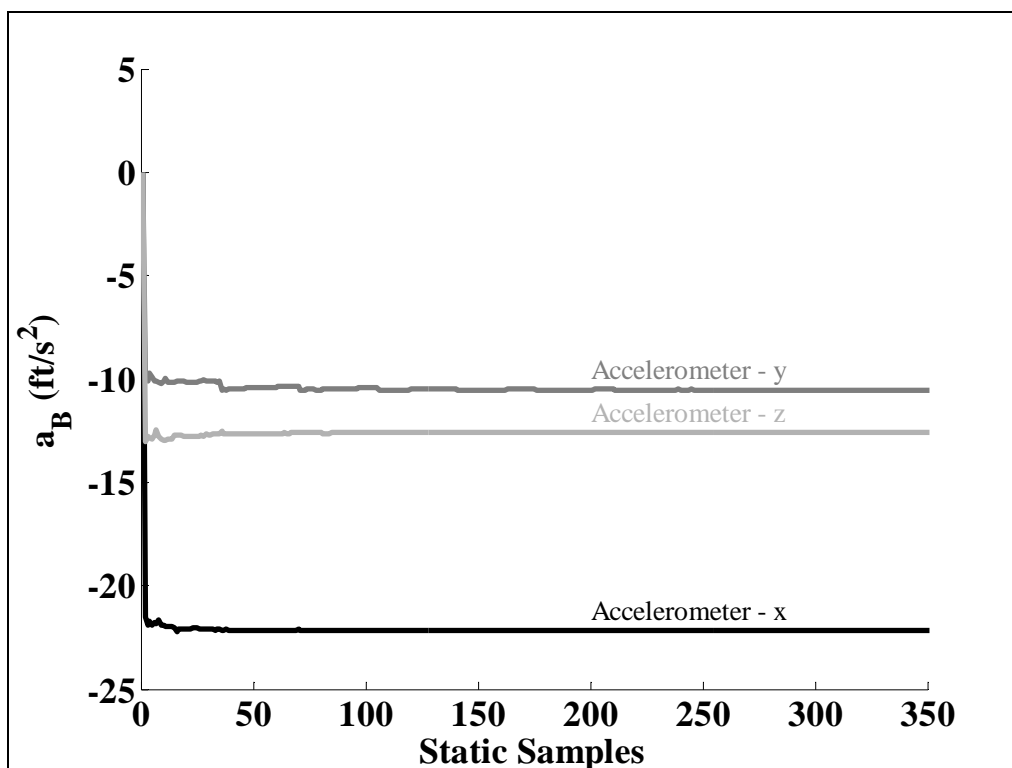


Figure 9. Accelerometer bias.

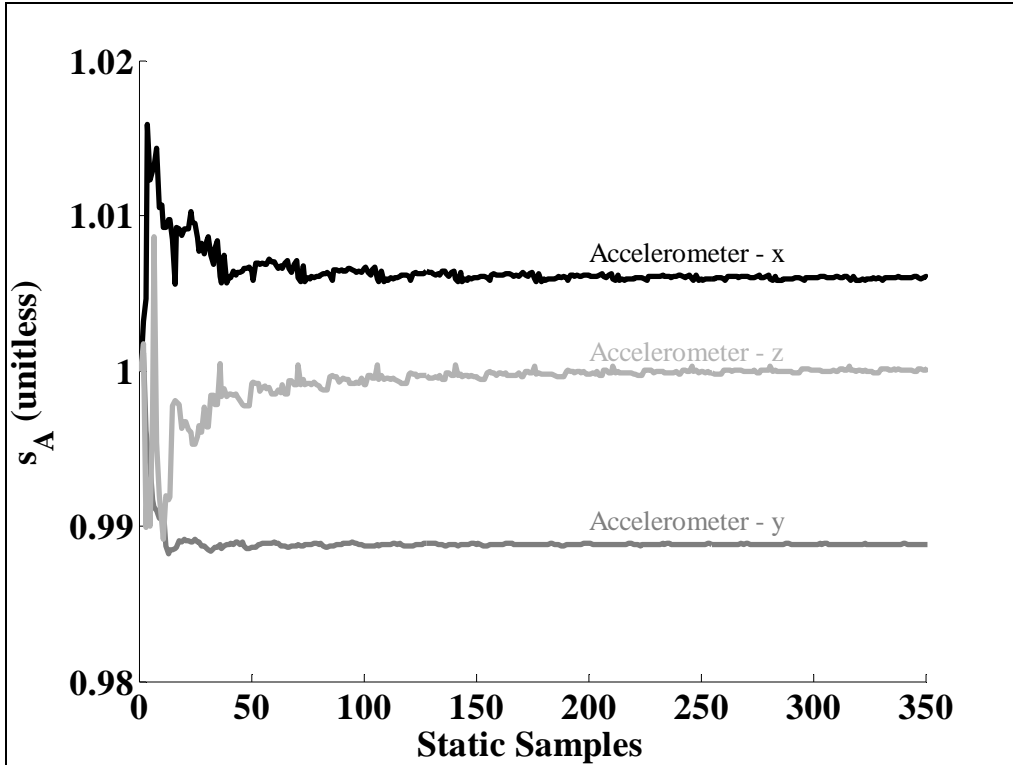


Figure 10. Accelerometer scale factors.

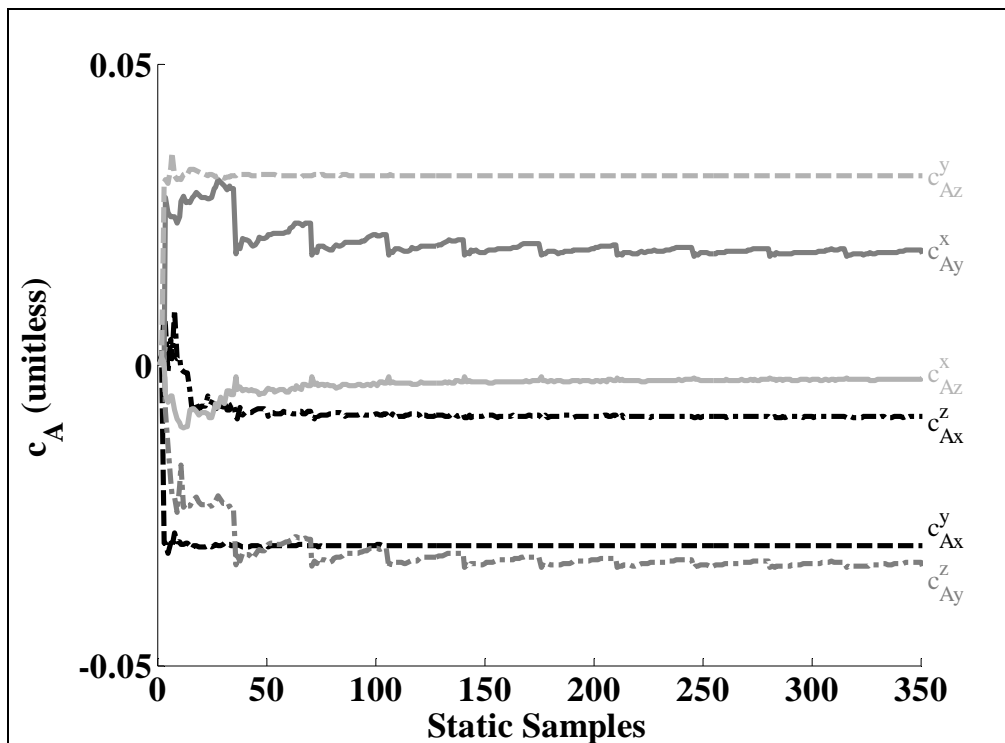


Figure 11. Accelerometer cross-axis sensitivities.

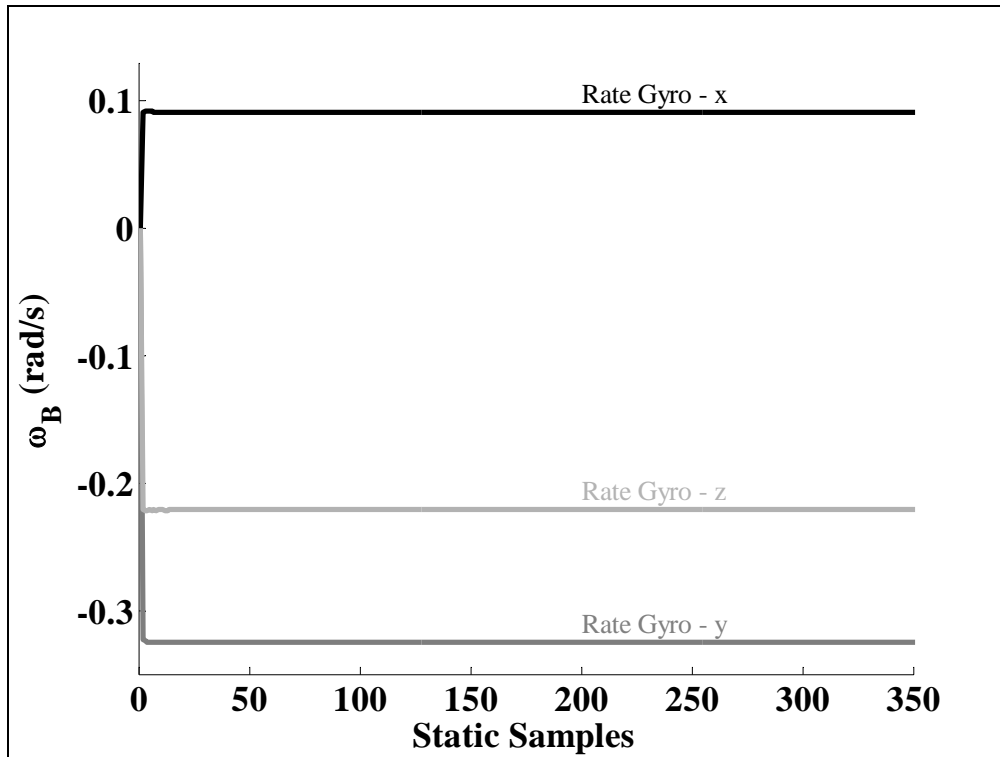


Figure 12. Rate gyro bias.

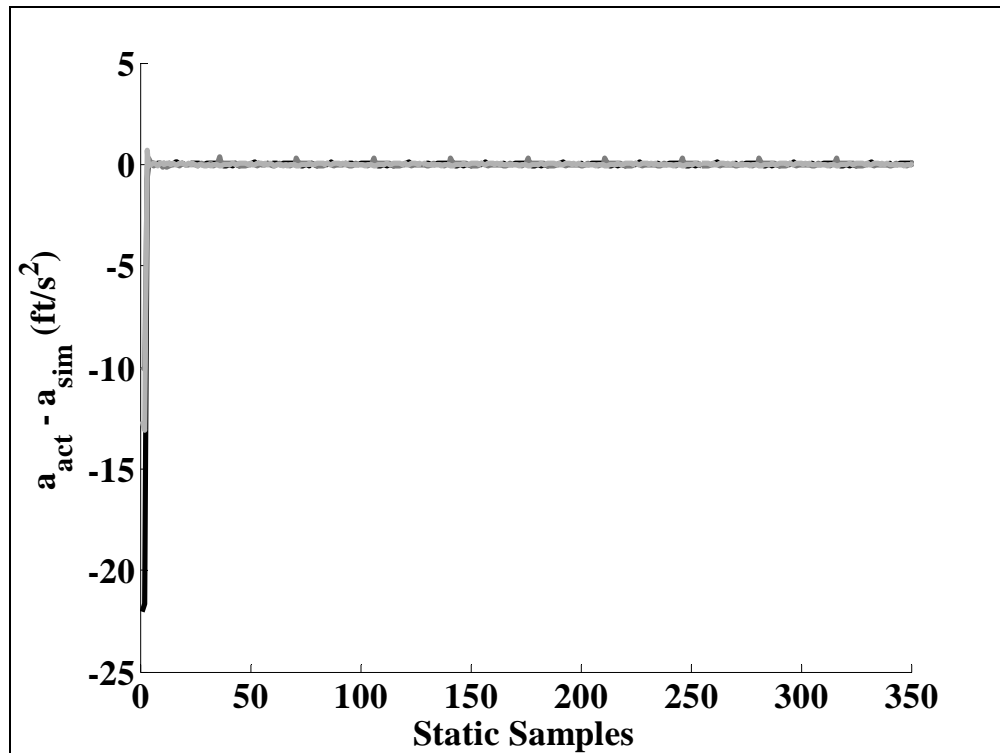


Figure 13. Static phase acceleration errors.

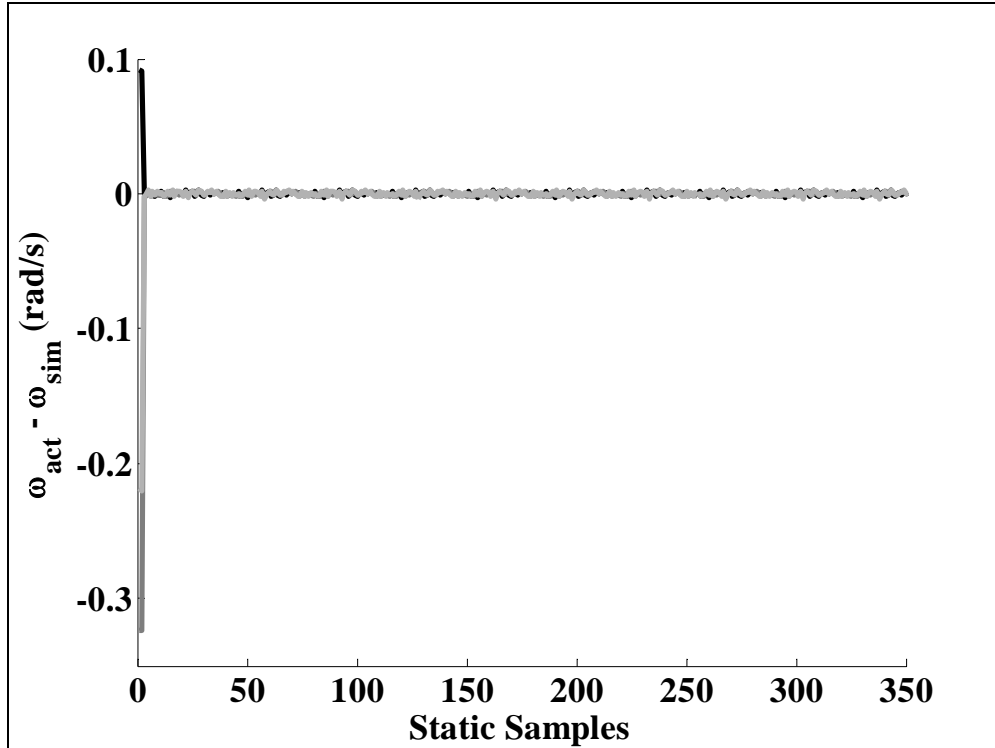


Figure 14. Static phase angular velocity errors.

Following the static phase, the static parameter values are fixed while accelerometer mispositions and gyroscope scale factors and cross-axis sensitivities are estimated from dynamic table motion. Ten sets of free vibration excitation data, each 5 s long, are stacked sequentially to create 50 s of data for parameter calibration. Sensor readings and position data are measured at a frequency of 500 Hz. The results of the dynamic phase of sensor calibration in figures 15–17 show that the dynamic phase allows convergence of the dynamic parameters. Sensor errors, plotted in figures 18 and 19, are consistent with the expected noise of the sensors after convergence.

To verify the accuracy of the estimation method, known parameter changes are introduced either physically or numerically. After calibrating the sensors based on new calibration the difference between the estimated parameters is compared with the expected change in error parameters. An analysis of table 2 shows that parameters are estimated consistently. When a known error is introduced the Kalman filter, tracks the error with excellent accuracy for scale factors and biases, the parameters that are varied electronically after data collection. The parameters that are varied by physically moving the sensors prior to data collection, misposition, and cross axis sensitivity, tracked within the tolerance of measurement. Due to the inherent difficulty of measuring positions and orientations of circuits mounted on a breadboard, a more precise comparison is not achievable with the current sensor arrangement.

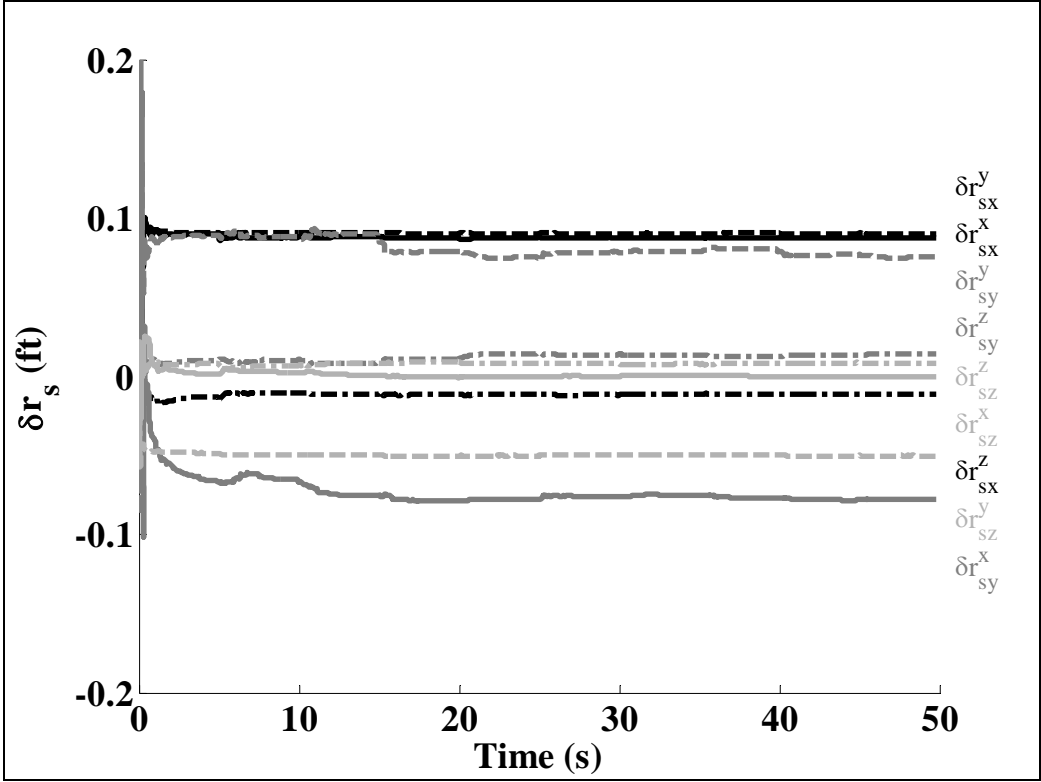


Figure 15. Accelerometer mispositions.

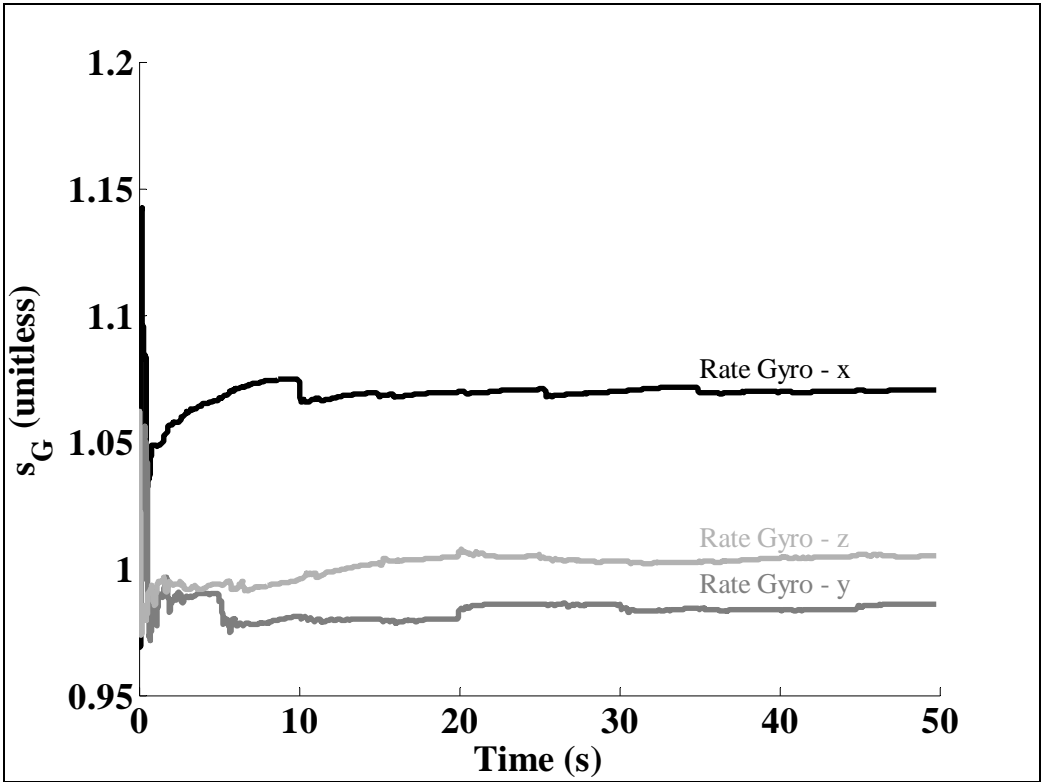


Figure 16. Rate gyro scale factors.

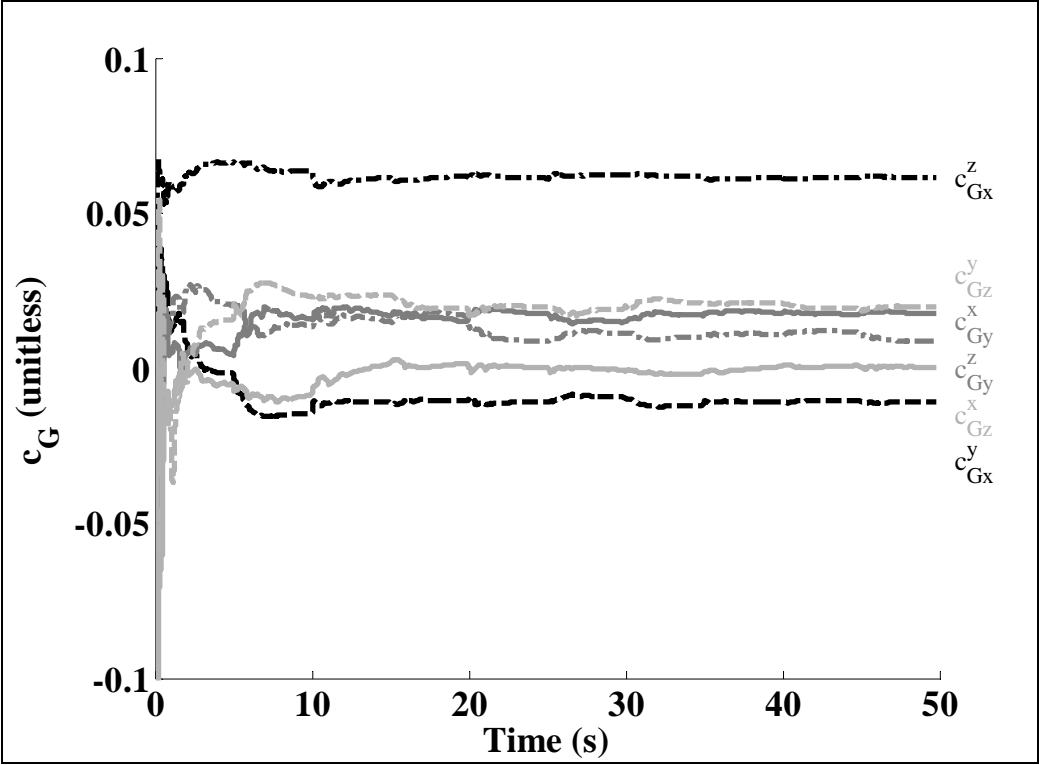


Figure 17. Rate gyro cross-axis sensitivities.

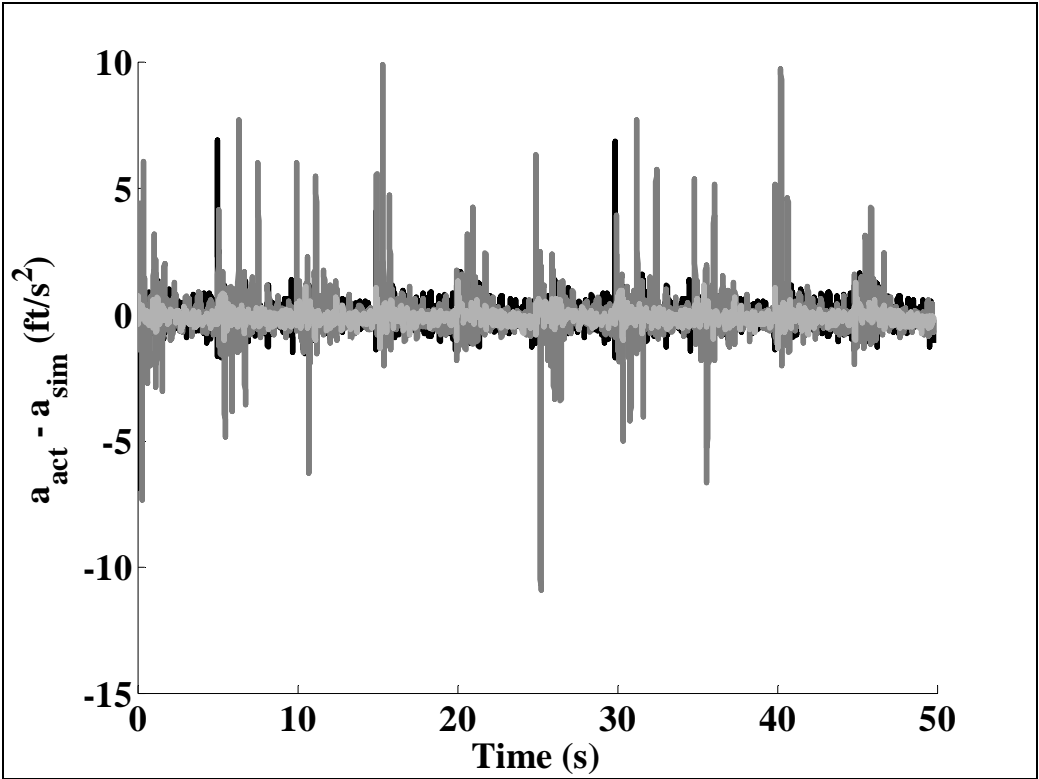


Figure 18. Dynamic phase acceleration errors.

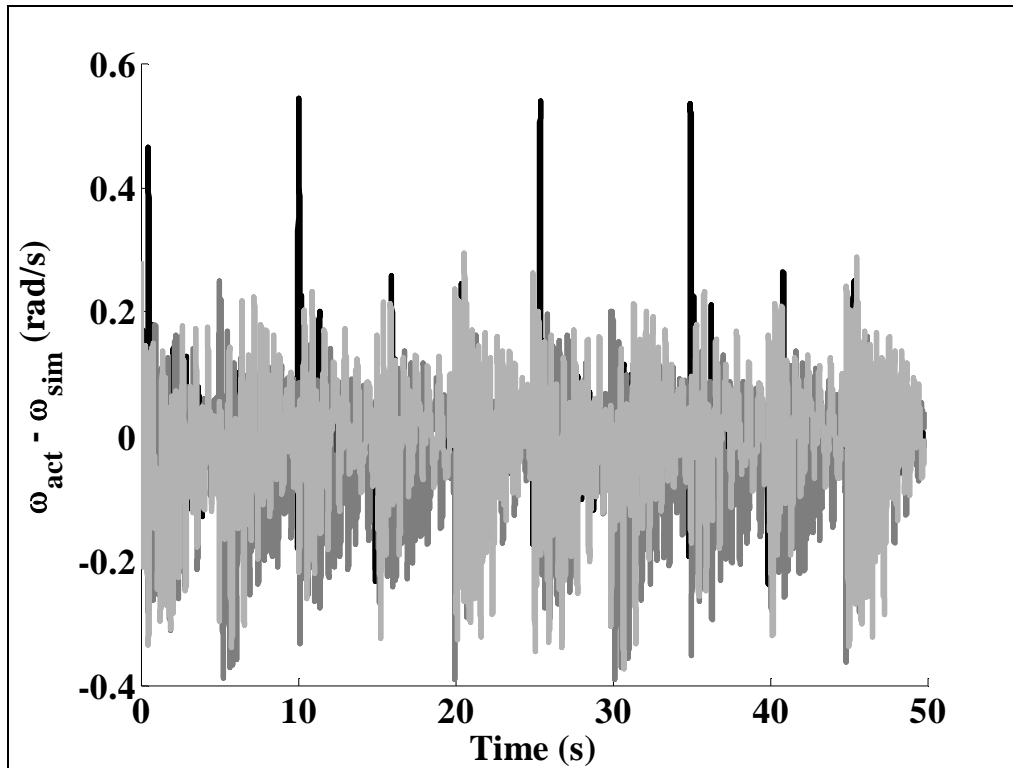


Figure 19. Dynamic phase angular velocity errors.

8. Conclusions

A relatively simple device for calibrating motion sensors onboard small robotic vehicles has been developed and validated through experimental testing. It was found that a two-stage static and dynamic procedure produced the most rapid estimates of motion sensor calibration parameters. This two-step estimation process isolates the effects of parameters that would otherwise be difficult to estimate simultaneously. For instance, during dynamic motion, the effects of accelerometer scale factor and misposition are very similar in sensor readings so the estimator has difficulty determining which parameter to update and subsequently neither parameter converges properly. The vibrating calibration table is conducive to a batch estimation process where many small robotic devices are attached to the table and simultaneously calibrated using the same motion sequence.

Table 2. Sensor error parameter comparison.

Parameter	Exp. Diff.	Diff.	Err.
a_{Bx} (ft/s ²)	20	19.782	-0.218
a_{By} (ft/s ²)	10	10.029	0.029
a_{Bz} (ft/s ²)	10	10.256	0.256
s_{Ax}	<i>1.1</i>	<i>1.099993</i>	<i>0.999993</i>
c_{Ax}^y (°)	-11.80	-11.66	0.14
c_{Ax}^z (°)	0.00	-1.20	-1.20
c_{Ay}^x (°)	0.00	0.71	0.71
s_{Ay}	<i>0.95</i>	<i>0.95</i>	<i>1</i>
c_{Ay}^z (°)	-10.30	-9.66	0.63
c_{Az}^x (°)	7.80	8.18	0.38
c_{Az}^y (°)	0.00	-0.84	-0.84
s_{Az}	<i>0.9</i>	<i>0.900006</i>	<i>1.000007</i>
δ_x^x (in)	-0.092	-0.127	-0.035
δ_x^y (in)	0.680	0.662	-0.018
δ_x^z (in)	-0.092	-0.123	-0.031
δ_y^x (in)	-0.742	-0.695	0.047
δ_y^y (in)	-0.030	-0.252	-0.222
δ_y^z (in)	0.742	0.822	0.080
δ_z^x (in)	-1.230	-1.060	0.171
δ_z^y (in)	0.000	0.055	0.055
δ_z^z (in)	0.057	-0.058	-0.114
ω_{Bx} (rad/s)	-0.1	-0.0995	0.0005
ω_{By} (rad/s)	0.3	0.2988	-0.0012
ω_{Bz} (rad/s)	0.2	0.1979	-0.0021
s_{Gx}	<i>0.95</i>	<i>0.950006</i>	<i>1.000007</i>
c_{Gx}^y (°)	0	0.50	0.50
c_{Gx}^z (°)	0	0.61	0.61
c_{Gy}^x (°)	0	0.51	0.51
s_{Gy}	<i>1.05</i>	<i>1.049992</i>	<i>0.999992</i>
c_{Gy}^z (°)	0	0.34	0.34
c_{Gz}^x (°)	0	0.19	0.19
c_{Gz}^y (°)	0	0.41	0.41
s_{Gz}	<i>1.1</i>	<i>1.099986</i>	<i>0.999987</i>

Note: Scale factor errors are multiplicative; all others are additive.

9. References

1. Costello, M.; Erickson, M. *Production Line Calibration for Sensors on Actively Controlled Bullets*; Oregon State University, May 2003.
2. Grewal, M. S.; Henderson, V. D.; Miyasako, R. S. Application of Kalman Filtering to the Calibration and Alignment of Inertial Navigation Systems. *IEEE Transactions on Automatic Control* **1991**, *36* (1), 4–12.
3. Kim, A.; Golnaraghi, M. F. Initial Calibration of an Inertial Measurement Unit Using an Optical Position Tracking System. *IEEE PLANS, Position Location and Navigation Symposium*, 2004, pp 96–101.
4. Leach, B.; Hui, K. In-Flight Technique for Calibrating Air Data Systems Using Kalman Filtering and Smoothing. *AIAA Atmospheric Flight Mechanics Conference and Exhibit*, August 2001.
5. Nebot, E.; Durrant-Whyte, H. Initial Calibration and Alignment of Low-Cost Inertial Navigation Units for Land Vehicle Applications. *Journal of Robotic Systems* **1999**, *16* (2), 81–92.
6. Haessig, D.; Friedland, B. Separate-Bias Estimation with Reduced-Order Kalman Filters. *IEEE Transactions on Automatic Control* **1998**, *43* (7), 983–987.
7. Hung, J. C.; Thacher, J. R.; White, H. V. Calibration of Accelerometer Triad of an IMU with Drifting Z-Accelerometer Bias. *Proceedings of the IEEE 1989 National Aerospace and Electronics Conference*, 1989, pp 153–158.
8. Ginsberg, J. H. *Advanced Engineering Dynamics*; 2nd ed.; Cambridge University Press: New York, 1998; pp 55–65.
9. Vicon Motion Systems Limited. *Vicon System Manual: VICON 612*; 12th ed., July 2002.
10. Analog Devices, Inc. *Low-Cost +/- 10 g Dual-Axis Accelerometer with Duty Cycle: ADXL210E*; 2002.
11. Analog Devices, Inc. *+/- 300°/s Single Chip Yaw Rate Gyro with Signal Conditioning: ADXRS300*; 2003.
12. Welch, G.; Bishop, G. An Introduction to the Kalman Filter. http://www.cs.unc.edu/~welch/kalman/kalman_filter/kalman.html (accessed March 2002). Department of Computer Science, University of North Carolina at Chapel Hill.

INTENTIONALLY LEFT BLANK.

List of Symbols, Abbreviations, and Acronyms

a_{Bi}	Bias of i^{th} accelerometer
a_i	Acceleration reading of i^{th} accelerometer
$\vec{a}_{Si/I}$	Acceleration of i^{th} accelerometer with respect to the ground
$\vec{a}_{\oplus/I}$	Acceleration of table center of mass with respect to the ground
b_f	Damping coefficient of the gimbal joint
c	Damping coefficient of the springs
c_{Ai}^j	Cross axis sensitivity of i^{th} accelerometer to the j^{th} direction
c_{Gi}^j	Cross axis sensitivity of i^{th} gyroscope to the j^{th} direction
C_k	Jacobian of the Kalman filter output equation
\vec{f}	Equations of motion for the dynamic system
g	Gravitational constant
$\vec{H}_{B/I}^{\oplus}$	Angular momentum of table with respect to the ground about the table mass center
I	Mass moment of inertia matrix of the table
k	Linear spring stiffness coefficient
k_t	Torsional spring stiffness coefficient
m	Mass of the table
P_k	Covariance matrix of the Kalman filter states
p, q, r	Components of angular velocity in the body frame
Q_k	System noise of the Kalman filter states
R	Rotation matrix from inertial frame to body frame
R_k	Covariance matrix of the Kalman filter measurements
R_s	Rotation matrix from body frame to sensor frame

$\vec{r}_{Fi \rightarrow P}$	Distance vector from i^{th} floor spring attachment point to pivot point
$\vec{r}_{P \rightarrow Si}$	Distance vector from pivot point to i^{th} accelerometer
$\vec{r}_{P \rightarrow Ti}$	Distance vector from pivot point to i^{th} table spring attachment point
$\vec{r}_{P \rightarrow \oplus}$	Distance vector from pivot point to table center of mass
$\vec{r}_{Ti \rightarrow Fi}$	Distance vector from i^{th} table spring attachment point to i^{th} floor attachment
s_{Ai}	Scale factor of i^{th} accelerometer
s_{Gi}	Scale factor of i^{th} gyroscope
s_o	Relaxed length of the springs
\vec{x}	State vector of the dynamic system
\hat{x}_k	Estimated Kalman filter states
v_k	Kalman filter measurement noise
z_k	Kalman filter measurements
$\vec{\alpha}_{B/I}$	Angular acceleration of table with respect to the ground
δ_{Si}^j	Misposition of i^{th} accelerometer in the j^{th} direction
ϕ, θ, ψ	Euler angles that define orientation of the table
ω_{Bi}	Bias of i^{th} gyroscope
$\vec{\omega}_{B/I}$	Angular velocity of table with respect to the ground
ω_i	Angular velocity reading of i^{th} gyroscope
$\vec{\omega}_{Si/I}$	Angular velocity of i^{th} gyroscope with respect to the ground
C_B	Vector component extraction operator for frame B
S_B	Skew symmetric cross product operator for frame B

NO. OF
COPIES ORGANIZATION

1 DEFENSE TECHNICAL
(PDF INFORMATION CTR
ONLY) DTIC OCA
8725 JOHN J KINGMAN RD
STE 0944
FORT BELVOIR VA 22060-6218

1 US ARMY RSRCH DEV &
ENGRG CMD
SYSTEMS OF SYSTEMS
INTEGRATION
AMSRD SS T
6000 6TH ST STE 100
FORT BELVOIR VA 22060-5608

1 INST FOR ADVNCD TCHNLGY
THE UNIV OF TEXAS
AT AUSTIN
3925 W BRAKER LN STE 400
AUSTIN TX 78759-5316

1 DIRECTOR
US ARMY RESEARCH LAB
IMNE ALC IMS
2800 POWDER MILL RD
ADELPHI MD 20783-1197

3 DIRECTOR
US ARMY RESEARCH LAB
AMSRD ARL CI OK TL
2800 POWDER MILL RD
ADELPHI MD 20783-1197

3 DIRECTOR
US ARMY RESEARCH LAB
AMSRD ARL CS IS T
2800 POWDER MILL RD
ADELPHI MD 20783-1197

ABERDEEN PROVING GROUND

1 DIR USARL
AMSRD ARL CI OK TP (BLDG 4600)

<u>NO. OF</u> <u>COPIES</u>	<u>ORGANIZATION</u>
1	US AIR FORCE RSRCH LAB MUNITIONS DIR AFRL/MNAV G ABATE 101 W EGLIN BLVD STE 219 EGLIN AFB FL 32542
1	OREGON STATE UNIV DEPT OF MECHL ENGRG M COSTELLO CORVALLIS OR 97331
1	CDR US ARMY ARDEC AMSTA AR CCH S MUSALI PICATINNY ARSENAL NJ 07806-5000
2	CDR US ARMY TANK MAIN ARAMAMENT SYSTEM AMCPM TMA D GUZIEWICZ C LEVECHIA PICATINNY ARSENAL NJ 07806-5000
1	CDR USARDEC AMSTA AR CCH A M PALATHINGAL PICATINNY ARSENAL NJ 07806-5000
1	CDR US ARMY RES OFC AMXRO RT IP TECH LIB PO BOX 12211 RESEARCH TRIANGLE PARK NJ 27709-2211
3	ARROW TECH ASSOC INC R WHYTE A HATHAWAY H STEINHOFF 1233 SHELBOURNE RD STE D8 SOUTH BURLINGTON VT 05403

<u>NO. OF</u> <u>COPIES</u>	<u>ORGANIZATION</u>
	<u>ABERDEEN PROVING GROUND</u>
24	DIR USARL AMSRD ARL HR SD T MERMAGEN AMSRD ARL WM EG E SCHMIDT AMSRD ARL WM B R COATES J NEWILL AMSRD ARL WM BA G BROWN B DAVIS T HARKINS T KOGLER D LYON S WANSACK M WILSON AMSRD ARL WM BC B GUIDOS P PLOSTINS (5 CPS) J SAHU S SILTON D WEBB P WEINACHT AMSRD ARL WM BF R PEARSON S WILKERSON AMSRD ARL WM TC R SUMMERS